HOSTED BY
ELSEVIER
Available online at www.sciencedirect.com
ScienceDirect
Soils and Foundations 65 (2025) 101625
SOILS AND FOUNDATIONS
www.elsevier.com/locate/sandf

Technical Paper

Effects of flocculants on in–situ recycling potential of waste EPB shield muck with residual foams

Yao Lu [a], Ming Huang [a,*], Jim S. Shiau [b], Fengwen Lai [a], Liqian Peng [c]

[a] School of Civil Engineering, Fuzhou University, Fuzhou 350108, China
[b] School of Engineering, University of Southern Queensland, Toowoomba 4350, Australia
[c] China Railway 18th Bureau Group First Engineering Co., Ltd, Baoding 072750, China

Received 5 November 2024; received in revised form 17 April 2025; accepted 21 April 2025
Available online 16 May 2025

Abstract

The in–situ recycling technique offers a promising solution for the efficient management of the escalating volumes of waste muck or slurry generated during shield tunneling. While foam is extensively utilized for soil conditioning in earth pressure balance (EPB) tunneling, the effects of organic and inorganic flocculants on the in–situ recycling potential of waste EPB shield muck containing residual foams remain underexplored. To bridge this gap, laboratory experiments were conducted using four flocculants: cationic polyacrylamide (CPAM), nonionic polyacrylamide (NPAM), anionic polyacrylamide (APAM), and polyaluminum chloride (PACL), with an enhanced flocculation and press–filtration apparatus. The defoaming–flocculation–dewatering behavior of waste EPB shield muck was systematically investigated by evaluating key parameters, including residual foam height, defoaming ratio, antifoaming ratio, total suspended solids, turbidity, moisture content, and zeta potential, while accounting for both muck dry mass and fines content. Moreover, the microscopic structure of flocculates and filter cakes was characterized using nanoparticle size analysis and scanning electron microscopy. The experimental results reveal that CPAM exhibits constrained flocculation and dewatering efficiency, primarily attributed to diminished charge neutralization resulting from residual anionic surfactants. In contrast, PACL demonstrates superior dewatering performance compared to NPAM and APAM, but exhibits the lowest flocculation and foam–suppression efficiency. Additionally, a consistent linear negative correlation is identified between the flocculation and dewatering indices of EPB shield muck, independent of the flocculant type, whether organic or inorganic.

Keywords: EPB shield; Flocculant; In–situ recycling; Residual foam; Waste muck

1. Introduction

Earth pressure balance (EPB) shield has been extensively utilized in the construction of urban metro tunnels owing to its high efficiency, safety, cost–effectiveness, strong adaptability to various strata, and compact operational footprint (Budach and Thewes, 2015; Li et al., 2022b; Zhang et al., 2020). Notably, over the past decade, more than 270 million cubic meters of muck have been generated from metro tunnel construction in China. However, the direct and efficient utilization of this waste muck is challenging due to its high moisture content and low mechanical strength (Lai et al., 2025; Zhang et al., 2024). Historically, the disposal of waste EPB shield muck primarily relied on abandonment or landfilling methods (Zhang et al., 2022a). These disposal practices not only contribute to environmental pollution and resource wastage but also pose significant geological hazards (Hu et al., 2022; Sun et al., 2023a; Zhang et al., 2022a,

* Corresponding author.
E-mail addresses: 220510021@fzu.edu.cn (Y. Lu), huangming05@fzu.edu.cn (M. Huang), Jim.Shiau@unisq.edu.au (J.S. Shiau), laifengwen@fzu.edu.cn (F. Lai).

https://doi.org/10.1016/j.sandf.2025.101625
0038-0806/

2022c). For instance, Yin et al. (2016) documented a severe landslide incident at a waste material landfill in Shenzhen, China, which resulted in 77 fatalities and the destruction of 33 houses. Recently, most landfills located outside urban areas in China have reached their maximum waste disposal capacities, thereby increasing security risks. Furthermore, regulations and governmental guidelines, such as the Muck Treatment Plan Draft issued by the Shenzhen Housing and Construction Bureau in 2021, mandate that only muck with a moisture content of less than 40 % by weight can be transported from construction sites to suburban areas for safe disposal.

To address the aforementioned challenges, in–situ recycling technology offers a promising solution for achieving eco–friendly, efficient, and large–scale resource utilization of waste shield muck (or slurry) (Wu et al., 2022; Zhou et al., 2017). Following sand separation, the disposal process for waste muck typically involves flocculation through the addition of flocculants and dewatering via mechanical pressure-filtration, particularly for fine–grained soils (Sun et al., 2023a, 2023b), as illustrated in Figs. 1 and 2. Numerous studies have investigated the flocculation and dewatering of waste muck and slurry (Cui et al., 2022; Doi et al., 2023; Najafabadi and Soares, 2021; Wang et al., 2019; Wu et al., 2022; Zhang et al., 2022b). The mechanisms by which flocculants influence flocculation and dewatering efficiencies have been comprehensively reviewed in Wei et al. (2018) and Michał et al. (2022). However, it is also important to highlight that soil conditioning during EPB shield tunneling is unavoidable to address various geological challenges, such as muck clogging and groundwater ingress (Budach and Thewes, 2015; Lu et al., 2024a; Wang et al., 2023). A key distinction between waste EPB shield muck and other waste slurries, such as those from slurry shields or pipe jacking, lies in the presence of residual foams, as discussed in Zhang et al. (2021) and Wu et al. (2022).

Fig. 1 demonstrates that the defoaming procedure is critical to prevent the formation of an upper foam layer in the muck pit (Fig. 1a–b), foam generated by water flow (Fig. 1c–d), foam–induced challenges in slurry pumping (Fig. 1e), and foam overflow in the flocculation tank (Fig. 1f). Consequently, compared to conventional in–situ recycling methods, the high–pressure water flow employed in preliminary and rolling screening is connected to a liquid tank by introducing defoamers at a specific dilution ratio using circulating water, as illustrated in Fig. 2. Based on the adsorption characteristics of foam liquid film reported in Li et al. (2022b), it can be inferred that the effects of residual foams primarily target fine–grained soils during the defoaming–flocculation–dewatering process. Although previous studies have examined the influence of defoamers and foaming agent components on the defoaming–flocculation–dewatering behavior of waste EPB shield muck (Lu et al., 2024b, 2024c, 2024d), the impact of organic and inorganic flocculants on the in-situ recycling potential, particularly in the presence of residual foams, remains insufficiently understood. As highlighted earlier, the inappropriate selection of flocculants due to their distinct physicochemical properties may significantly compromise the defoaming–flocculation–dewatering efficiency of waste EPB shield muck.

This study investigates the defoaming–flocculation–dewatering behavior of waste EPB shield muck using four flocculants: cationic, nonionic, and anionic polyacrylamides, and polyaluminium chloride, through a series of

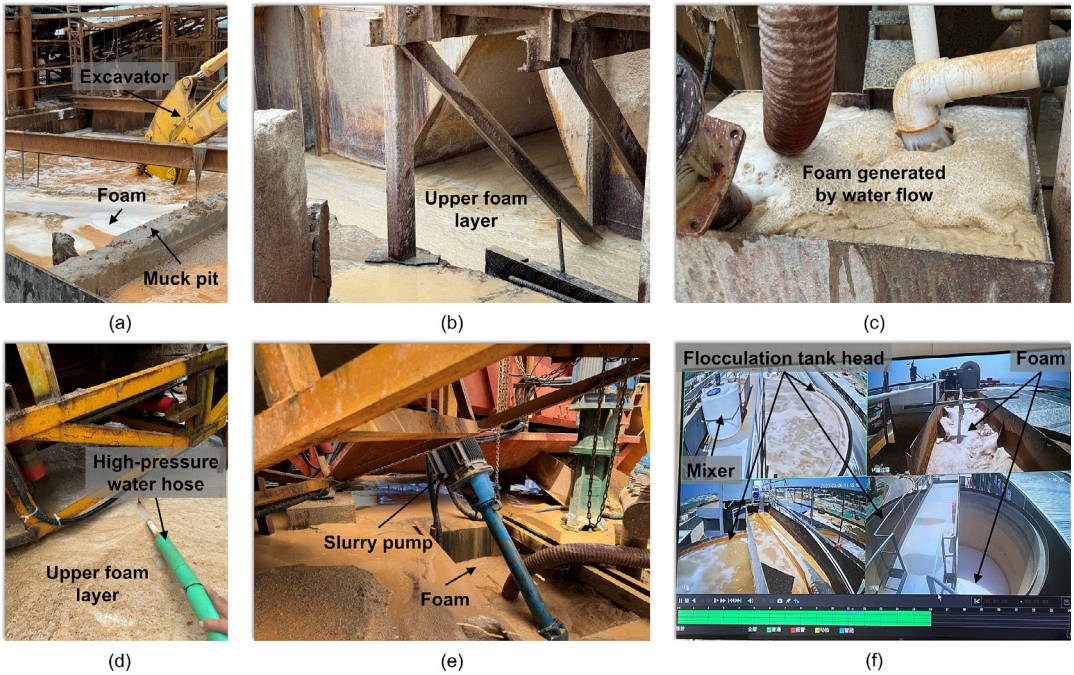

Fig. 1. (a)–(b) Upper foam layer in the muck pit, (c)–(d) foam generated by water flow, (e) foam in the slurry pit, and (f) foam in the flocculation tank.

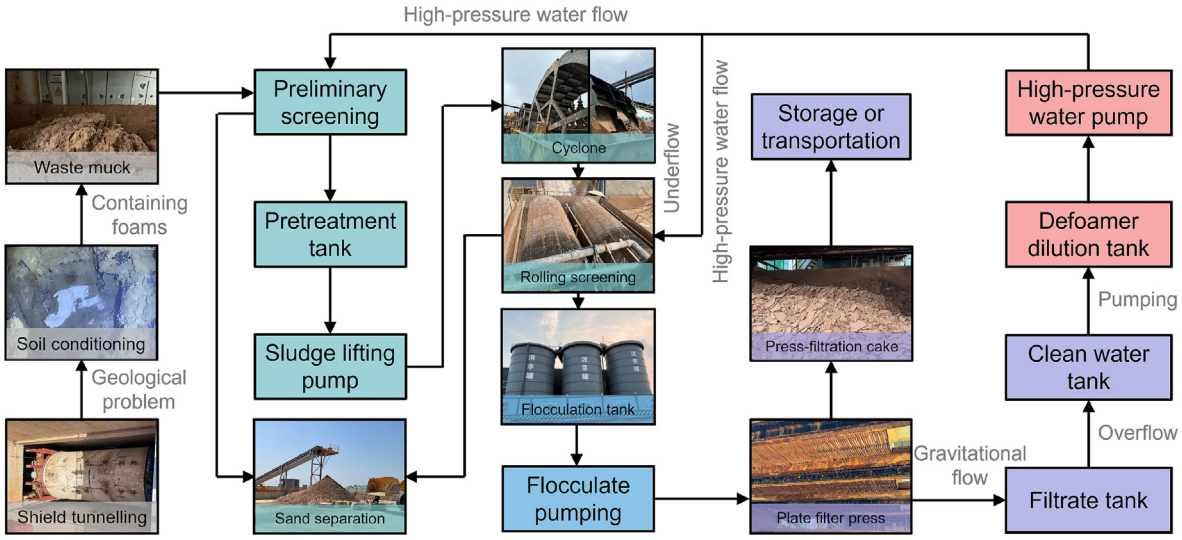

Fig. 2. In–situ recycling procedure of EPB shield waste muck.

experiments conducted with an improved laboratory flocculation and filterpress apparatus. Key performance indices, including residual foam height, 5–minute defoaming ratio, 30–minute antifoaming ratio, total suspended substances, turbidity, moisture content, and zeta potential, were systematically evaluated. For nonionic polyacrylamide and polyaluminium chloride, the impacts on muck dry mass and fines content were also examined. Additionally, nanoparticle size analysis and scanning electron microscopy were employed to analyze flocculate structures and press–filtration cakes, providing deeper insights into the underlying mechanisms. The findings offer a detailed understanding of the interactions between flocculants and EPB shield muck components, enabling the optimization of flocculant selection and operational parameters for improved dewatering efficiency.

2. Background

An engineering case, specifically the section between Shuanghu Station and Airport Economic Zone Station of the Xiamen Metro Line–3 Project in southeastern Fujian Province, China, is illustrated in Fig. 3a and b. This section is primarily excavated using two EPB shield machines with a diameter of 6.98 m. The left– and right–line lengths are 2283.042 m and 2305.759 m, respectively. Based on the geological survey report, the properties of the main strata, including granite residual soil, completely decomposed granite, and strongly decomposed granite excavated by EPB shield tunneling are summarized in Table 1. It is evident that the content of fine–grained sands to large boulders exceeds 60 % by weight (abbreviated as wt% hereafter) for all three excavation formations, as per ISO 14688–1 (2017a) and GB/T 50145 (2007). Based on the liquidity index (I_L), it can be inferred that the undisturbed soils are very stiff (ISO 14688–2, 2017b). The high content of coarse–grained soils presents significant additional economic benefits for the project team, which, alongside environmental considerations, is a key factor influencing the decision to adopt an in–situ recycling scheme for waste EPB shield muck.

As depicted in Fig. 2, the sand and gravel particles separated from the muck using equipment such as rolling screens and sand washing machines are directly utilized as construction building materials. The remaining waste slurry, after the addition of defoamers and flocculants, is pumped into a plate filter press for dewatering. Ultimately, it is transformed into pressure–filtration cakes with low moisture content, meeting the water content limit required for transporting waste muck off the construction site (Hu et al., 2022; Sun et al., 2023a, 2023b; Wu et al., 2022).

In the case of Xiamen Metro Line–3, a detailed analysis of equipment capacity and economic benefits is presented in Table 2. As shown, the cost of reusing EPB shield muck would save at least 13.29 million RMB compared to traditional landfilling methods. Additionally, the resulting pressure–filtration cakes are easier to store and transport. In–situ recycling methods can effectively mitigate environmental pollution caused by waste muck leakage during transportation. Recently, numerous researchers have explored various resource utilization methods for pressure–filtration cakes, such as their use in synchronous grouting materials, high–belite cementitious materials, and unfired bricks (Hu et al., 2022; Wu et al., 2022; Zhang et al., 2020, 2022a, 2022c, 2024; Zhou et al., 2017). However, the selection of appropriate flocculants remains a critical challenge for achieving high–efficiency in–situ recycling of waste EPB shield muck containing residual foams, particularly in the defoaming–flocculation–dewatering processes of fine–grained soils after sand separation. It is essential to elucidate the interaction mechanisms between flocculants and other components, such as fines content, foaming agents, and defoamers, to provide valuable insights for practical engineering applications.

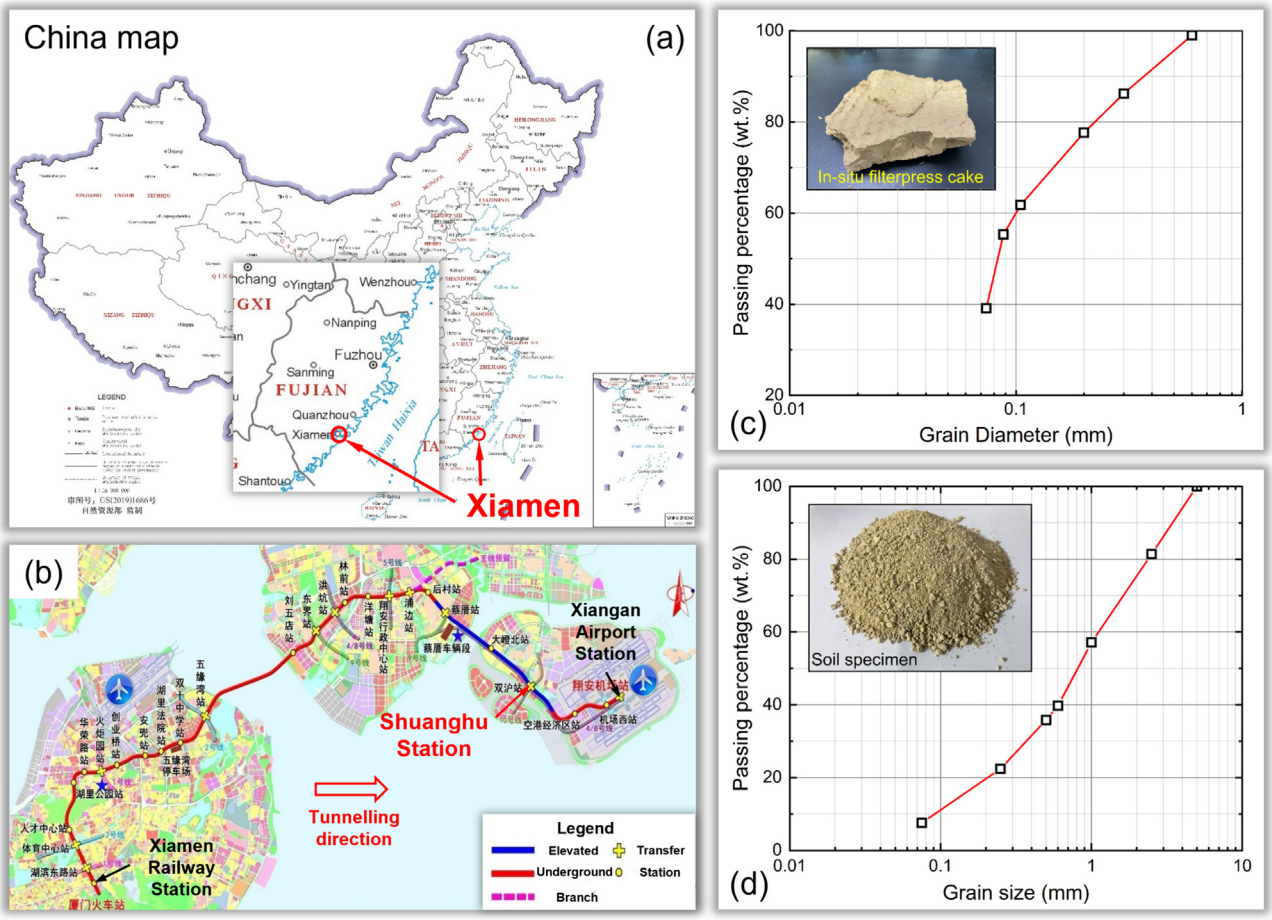

Fig. 3. (a) and (b) Site taken soil from Shuanghu Station of Xiamen Metro Line–3, (c) grain size distribution of field fiterpress cakes, and (d) grain size distribution of testing soil specimens.

Table 1
Soil parameters from geological survey report for Xiamen Metro Line–3.

Soil type	Natural gravimetric water content (w_n; wt%)	Natural void ratio (e)	Liquidity index (I_L)	Plasticity index (I_P)	Mass percentage (wt%)				
					>2 mm	>0.5 to ≤2 mm	>0.25 to ≤0.5 mm	>0.075 to ≤0.25 mm	≤0.075 mm
Granite residual soil	14.1–51.1	0.41–1.56	−0.78–0.52	8.60–19.50	24.3	32.4	12.3	18.2	12.8
Completely decomposed granite	19.3–47.1	0.60–1.33	−0.60–0.49	10.10–34.90	25.3	21.8	8.1	11	33.8
Strongly decomposed granite	17.9–35.5	0.56–1.05	−0.78–0.36	6.70–19.40	26.4	21.2	8.4	11.2	32.8

Table 2
Equipment capacity and economic benefits in terms of Xiamen Metro Line–3.

Term	Volume (m^3)			Unit price (RMB/m^3)	Total price (million RMB)
	Average production per day	Daily processing capacity	Gross amount		
Muck recycling	2895	3000	420,000	67.35	28.29
Filter cake transported off the site	105,000			80	8.40
Filter cake used in the field	105,000			/	/
Sand and gravel sales	168,000			97.5	16.38
Tunnel muck directly transported off the site	420,000			80	33.60

3. The experiment

3.1. Materials

As outlined above, this paper specifically investigates the effects of organic and inorganic flocculants on the defoaming–flocculation–dewatering characteristics of fine–grained soils following sand separation. Initially, the grain size range of the test fine–grained soils was determined based on field pressure–filtration cakes collected from the Xiamen Metro Line–3 Project. After drying, crushing, and sieving, the grain size distribution curve is illustrated in Fig. 3c. As shown, the grain size is less than 0.6 mm, with the fines content (FC; < 0.075 mm) ranging from 30 to 40 wt% (GB/T 50145). The test soil specimens were obtained from the launch shaft of the EPB shield machine at Shuanghu Station of Xiamen Metro Line–3. It is important to note that these soil specimens did not contain foaming agent components, as the shaft was excavated using a cut–and–cover method. Their grain size distribution curve, obtained through a similar measurement procedure, is depicted in Fig. 3d. The mineral compositions of the pressure–filtration cakes and soil specimens were analyzed using energy dispersive spectroscopy (EDS) and X–ray diffraction (XRD), as summarized in Table 3. The results revealed that the predominant clay mineral in both samples was kaolinite, accounting for 78.6 wt% in the field pressure–filtration cakes and 67.4 wt% in the test soil samples, respectively.

Based on the principles of versatility and effectiveness, the organic flocculants cationic polyacrylamide (CPAM), nonionic polyacrylamide (NPAM), and anionic polyacrylamide (APAM), each with a molecular weight of ≥ 10 million, were selected (Wu et al., 2022). For comparative analysis, the inorganic flocculant polyaluminium chloride (PACL) with a purity of ≥ 28 wt% was also chosen. The specific parameters of these four flocculants are detailed in Table 4.

As reported by Li et al. (2022b) and Lu et al. (2024a), the foaming agents used in real tunnel construction typically consist of anionic/nonionic surfactants and foam stabilizers. Among these, the foam stabilizer primarily functions to reduce foam volume, water drainage rate, and average pore diameter while enhancing foam stability (Wei et al., 2020). Through field investigations conducted on the Xiamen Metro Line–3 project, it was determined that the foaming agent used comprised anionic surfactant sodium fatty alcohol polyoxyethylene ether sulfate (AES), nonionic surfactant alkyl polyglycoside (APG), and foam stabilizer sodium carboxymethyl cellulose (CMC). Consequently, in this study, AES, APG, and CMC were employed to simulate the residual foaming agent components, as detailed in Table 4.

Previous work by the authors demonstrated that a hydroxyl silicone oil–glycerol polyoxypropylene ether (H–G) defoamer, specifically developed for waste EPB shield muck, exhibited superior defoaming and antifoaming efficiencies compared to several commercial defoamers (Lu et al., 2024d). As an oil–solid compound defoamer, it was classified as a fast defoamer, as described by Denkov et al. (2014), and was utilized in this study (see Table 4).

3.2. Specimen preparation

In the experiments, soils with a grain size of < 0.6 mm were used, consistent with the grain size distribution of

Table 3
XRD analysis of mineral components.

Sample	Mineral name	Sericite	Sanidine	Kaolinite	Quartz	Orthoclase
	Chemical formula	$Ti_{0.02}Si_{3.128}O_{12}Na_{0.17}Mg_{0.022}K_{0.727}Fe_{0.032}Ca_{0.011}Al_{2.75}H_2$	$Si_{12}O_{32}Na_{0.56}K_{3.44}Al_4$	$Si_4O_{18}Al_4H_8$	SiO_2	$Al_{0.97}Ba_{0.005}Ca_{0.009}K_{0.931}Na_{0.055}O_8Si_{3.03}$
Pressure filtration cake	Mass percentage (wt%)	8.4	6.2	78.6	6.8	/
Testing soil	Mass percentage (wt%)	5.0	/	67.4	/	27.6

Table 4
Parameters of testing additives.

Contributions	Materials	Type	Parameter	Abbreviation
Residual foaming agent components	Anionic surfactant	Sodium fatty alcohol polyoxyethylene ether sulfate	≥ 70 wt%	AES
	Nonionic surfactant	Alkyl polyglycoside	≥ 70 wt%	APG
	Foam stabilizer	Sodium carboxymethyl cellulose	≥ 95 wt%	CMC
Defoaming and antifoaming	Defoamer	Hydroxyl silicone oil–glycerol polyoxypropylene ether	Self–synthesis	H–G
Flocculation and dewatering	Flocculant	Polyaluminium chloride	≥ 28 wt%	PACL
		Cationic polyacrylamide	≥ 10 million	CPAM
		Nonionic polyacrylamide	≥ 10 million	NPAM
		Anionic polyacrylamide	≥ 10 million	APAM

field pressure–filtration cakes. The soil specimens were further sieved into coarse–grained soils (>0.075 to ≤0.6 mm) and fine–grained soils (≤0.075 mm). The residual content of AES in waste EPB shield muck from the Xiamen Metro Line–3 was measured at 0.156 wt%, as reported by Lu et al. (2024d). Consequently, a test concentration of 0.2 wt% for AES was selected, with the same concentration applied to APG. Based on the ratio of foam stabilizers (polymers) to surfactants reported by Li et al. (2022b) and Lu et al. (2024d), the concentration for CMC was set at 0.02 wt%. As suggested by Denkov et al. (2014) and Lu et al. (2024d), a dosage of 0.002 wt% was used for H–G. It is important to note that the influence of foaming agent components and defoamers has been explored by Lu et al. (2024b), and the concentrations of AES, APG, CMC, and H–G in this study were maintained at constant values across all experiments.

The effects of flocculants on defoaming–flocculation–dewatering behavior were investigated using dosages of 0.00 (as a blank control group), 0.02, 0.04, 0.06, 0.08, and 0.10 wt% for APAM, CPAM, NPAM, and PACL (Qin et al., 2023; Sun et al., 2023b). During these tests, the muck dry mass (MDM) and fines content (FC; < 0.075 mm) were maintained at 10 and 30 wt%, respectively.

The impact of MDM (i.e., initial water content) on defoaming–flocculation–dewatering performance was evaluated by varying the MDM at 5, 10, 15, 20, 25, and 30 wt %. The dosages of the selected organic and inorganic flocculants were held constant, while the FC was fixed at 30 wt%.

The influence of FC on defoaming–flocculation–dewatering characteristics was analyzed by adjusting the FC to 0, 10, 20, 30, 40, and 50 wt% to simulate different excavation strata encountered in real tunnel projects. The dosages of the selected flocculants remained unchanged, and the MDM was consistently maintained at 10 wt%.

All experiments were repeated three times to minimize the effects of operational errors, and the average values were recorded as the final results, as summarized in Table 5.

3.3. Apparatus and procedure

3.3.1. Test apparatus

The improved laboratory flocculation and dewatering apparatuses utilized in these experiments are illustrated in Fig. 4, with detailed descriptions provided in the authors' previous publications (Lu et al., 2024b, 2024d). For context, Fig. 2 depicts the in–situ flocculation tank at Xiamen Metro Line–3, which has an inner diameter of 8 m and a height of 12 m. In this study, a laboratory–scale model of the flocculation tank was developed with a geometric similarity ratio of 1/50, as shown in Fig. 4 (Steps 1 to 5). This design aligns with dimensions reported by Acosta-Santoyo et al. (2020). The flocculation apparatus, featuring a thickness of 0.5 cm, an inner diameter of 16 cm, and a height of 24 cm, includes a scaled flocculation tank with a scale and a mixer capable of maintaining a constant rotation speed. This setup simulates the dynamic deforming and flocculation processes encountered in practical scenarios, offering a more realistic alternative to the static settling column tests commonly reported in studies such as those by Li et al. (2022a), Najafabadi and Soares (2021), and Qin et al. (2023). Compared to a static settling column test, the flocculation efficiency and floc structure in the present device may be influenced by key parameters such as stirring speed and tank size.

Lu et al. (2024d) have defined quantitative indices for defoaming and antifoaming to evaluate the performance of different defoamers for waste shield muck. Following the definitions, in this study, the indices of 5–minute defoaming ratio (*DFR*; % by volume, abbreviated as vol % in the following) and 30–minute antifoaming ratio (*AFR*; vol%) were used to quantitatively characterize the efficiency of foam suppression.

Fig. 4 (Step 6) illustrates an improved laboratory filter-press apparatus, which incorporates a filter cloth comparable to that used in the Xiamen Metro Line–3. As detailed in Lu et al. (2024d), the apparatus consists of an air–pressure chamber and a filtrate chamber. A constant air pressure supply from the air compressor was maintained using a

Table 5
Programme of defoaming–flocculation–dewatering tests.

Types of flocculants	Dosages of flocculants (wt%)	MDM (wt%)	FC (wt%)	H–G (wt%)	AES (wt%)	APG (wt%)	CMC (wt%)	Number of tests
APAM	0.00; 0.02; 0.04; 0.06; 0.08; 0.10	10	30	0.002	0.02	0.2	0.2	18
NPAM	0.00; 0.02; 0.04; 0.06; 0.08; 0.10	10	30					18
CPAM	0.00; 0.02; 0.04; 0.06; 0.08; 0.10	10	30					18
PACL	0.00; 0.02; 0.04; 0.06; 0.08; 0.10	10	30					18
NPAM	0.02	5; 10; 15; 20; 25; 30	30					18
PACL	0.08	5; 10; 15; 20; 25; 30	30					18
NPAM	0.02	10	0; 10; 20; 30; 40; 50					18
PACL	0.08	10	0; 10; 20; 30; 40; 50					18

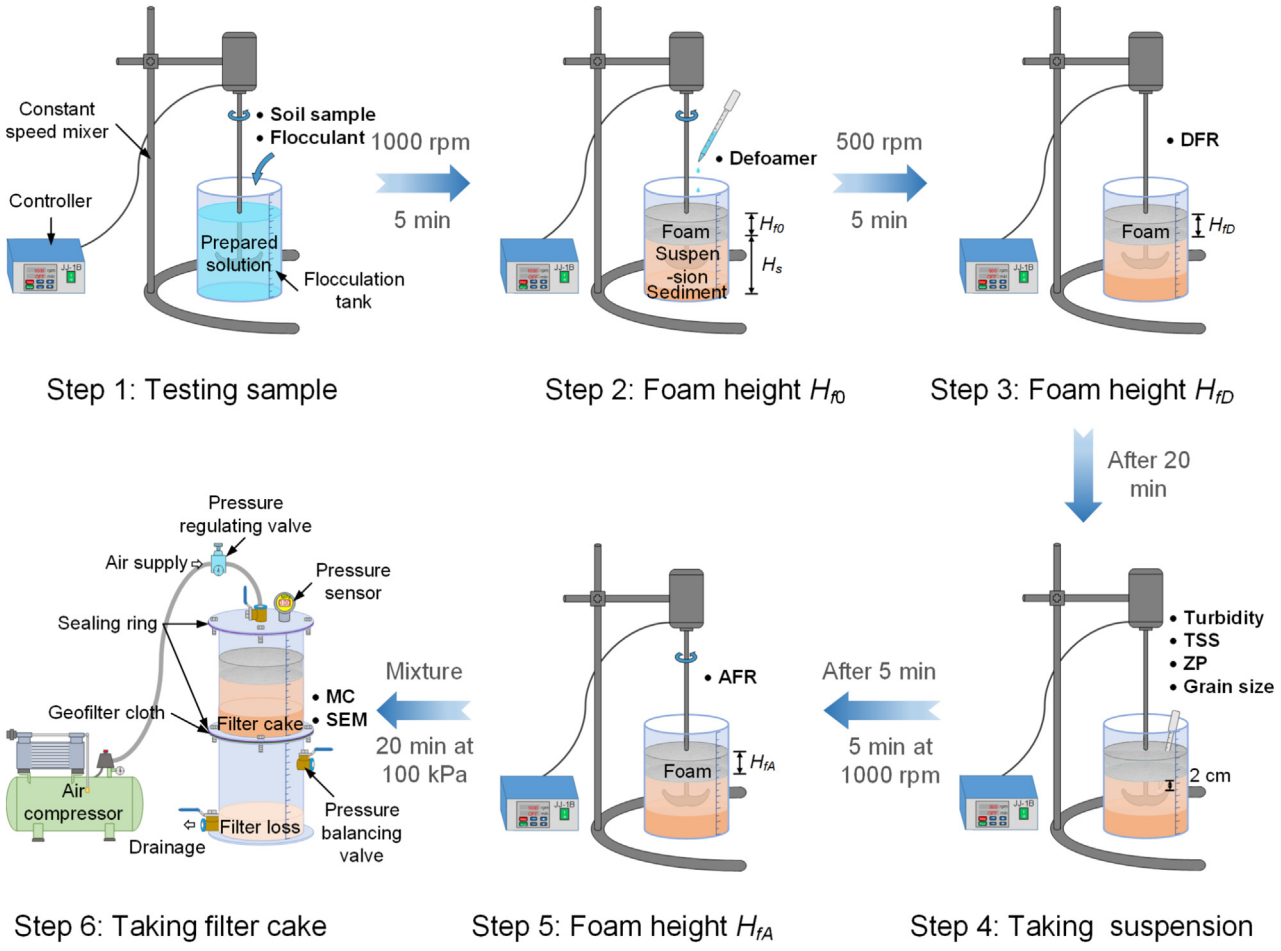

Fig. 4. Scheme of laboratory defoaming–flocculation–dewatering experiments.

pressure regulator and sensor installed on the air–pressure chamber. Doi et al. (2023) have investigated the effects of polymer flocculants on the dewatering behavior of clay–rich coal tailings using pressure filtration at an air pressure of 80 kPa and a resident time of 3 h. In line with the methodology reported by Doi et al. (2023), the air pressure and its residence time were consistently controlled at 100 kPa and 20 min, respectively, for all experiments, as the influence of mechanical parameters falls outside the scope of this study. The moisture content (*MC*; wt%) of the press–filtration cakes on the filter cloth within the air–pressure chamber was used as a key index to quantitatively evaluate the dewatering performance.

A portable turbidimeter (ZD–10A, China) was utilized to measure the turbidity index (NTU), which served as a qualitative indicator of flocculation efficiency by assessing the concentration of micro soil particles in the upper suspension.

Following the methodology of Konig et al. (2012), a 47–mm glass fiber membrane (China) with a pore diameter of 0.45 μm, dried at 105 °C for 1 h, was employed to determine the total suspended solids (*TSS*; g/L) concentration, providing a quantitative measure of flocculation efficiency.

The nanoparticle size and zeta potential (*ZP*) were measured using a Zetasizer Pro analyzer (Malvern Panalytical Ltd, UK) to further elucidate the microstructural characteristics of the flocs in the suspension. The zeta potential has been established as a critical parameter for evaluating the dewatering performance of slurry (Wang et al., 2019).

The microstructure of pressure–filtration cake pieces was visually examined using a field emission scanning electron microscope (FESEM; Nova NanoSEM 230, USA) after the samples were dried in an oven.

3.3.2. Test procedure

The procedure for conducting laboratory defoaming–flocculation–dewatering tests on waste EPB shield muck containing residual foams is outlined as follows:

Step 1: The soil specimens were combined with the flocculant and water at a specified mass ratio, as detailed in Table 5. This mixture was then stirred at 1000 rpm for 5 min.

Step 2: After allowing the mixture to stand for 2 min, a stratified phenomenon became apparent, with an upper foam layer, a middle suspension layer, and a lower sediment layer identifiable. The initial height of the foam layer

(H_{f0}) was recorded using the scale on the flocculation tank model (see Fig. 4; the same applies below). The defoamer was then titrated into the center of the foam surface, and the mixture was stirred at 500 rpm for 5 min, referencing the fast–stirring speed of 536 rpm used in the study by He et al. (2024).

Step 3: The foam height (H_{fD}) was recorded to calculate the 5–minute *DFR* (see Eq. (1), as defined in Lu et al. (2024b, 2024d). The mixture was subsequently allowed to stand for an additional 20 min.

$$DFR = \frac{H_{f0} - H_{fD}}{H_{f0}} \times 100 \quad (1)$$

Step 4: Suspension samples with a volume of 30 mL were collected from a depth of 2 cm below the liquid surface, consistent with the methodology described by Sun et al. (2023a). These samples were used to measure turbidity, *TSS*, *ZP*, and nanoparticle size of the flocs. It is important to note that the minor liquid loss incurred during sampling was not considered to significantly impact subsequent steps, as it represented a negligible proportion of the total mixture volume.

Step 5: After allowing the mixture to stand for an additional 5 min, it was stirred again at 1000 rpm for 5 min. The foam height (H_{fA}) was then recorded to calculate the 30–minute *AFR* (see Eq. (2), as defined by Lu et al. (2024b, 2024d).

$$AFR = \frac{H_{f0} - H_{fA}}{H_{f0}} \times 100 \quad (2)$$

Step 6: Finally, the mixture was poured into the upper air–pressure chamber of the filterpress device, and the air pressure was maintained at 100 kPa for 20 min. Pressure–filtration cakes weighing 100 g were collected from the center of the filter cloth to measure the *MC*. These samples were then dried at 105 °C for 24 h. The dried samples were precisely cut into cubes approximately 3 mm in length using a geo–cutter for subsequent SEM observation.

4. Results and discussion

4.1. Effects of organic and inorganic flocculants on defoaming–flocculation–dewatering characteristics

Fig. 5 illustrates the effects of four flocculants, APAM, CPAM, NPAM, and PACL, with mass contents (C_w, the ratio of additive mass to total mixture mass) ranging from 0.02 to 0.10 wt% on defoaming–flocculation–dewatering indices (10 wt% MDM, 30 wt% FC, 0.2 wt% AES, 0.2 wt % APG, 0.02 wt% CMC, 0.002 wt% H–G). As shown in Fig. 5a, the foam height (H_f) and liquid level height (H_s) exhibits no significant change with increasing PACL and CPAM, while both H_f and H_s gradually decrease with higher dosages of NPAM and APAM. The reduction trend is slightly more pronounced for NPAM compared to APAM, indicating better bubble suppression in practical applications. This behavior is attributed to the ability of NPAM and APAM, as polymers, to adsorb fine soil particles onto foam films due to surface charges (Doi et al., 2023), while their hydrophilic groups interact with free water molecules, converting them into bound water (Li et al., 2022b).

The *DFR* decreases with increasing dosages of PACL and NPAM, whereas for CPAM and APAM, it exhibits a three–stage trend: initial decrease, followed by an increase, and finally leveling off or declining again (see Fig. 5b). The *AFR* for PACL remains consistently at 0, while it slightly improves with higher CPAM dosages (see Fig. 5c). For NPAM and APAM, the *AFR* initially increases significantly to a peak before decreasing. These variations in *DFR* and *AFR* are primarily due to the thickening effect of the foam liquid film caused by the adsorption of clay particles and polymers. As a reference, Denkov et al. (2014) also noted that anionic and nonionic surfactants, along with polymers in foaming formulations, tend to adsorb onto solid particle surfaces, forming a hydrophobic layer and thereby exhibiting foam suppression activity.

As shown in Fig. 5d, the *TSS* gradually decreases until reaching a critical dosage for PACL (0.08 wt% C_w, 0.13 g/L *TSS*, 73.91 wt% *MC*, −27.97 mV *ZP*), NPAM (0.02 wt% C_w, 0.09 g/L *TSS*, 100.37 wt% *MC*, −56.8 mV *ZP*), and APAM (0.04 wt% C_w, 0.02 g/L *TSS*, 121.17 wt % *MC*, −44.4 mV *ZP*), after which it begins to rise. In contrast, *TSS* shows a continuous decline with increasing CPAM dosage, suggesting an unachieved critical CPAM dosage in this experiment. Notably, *MC* trends are opposite to *TSS* for all flocculants, including organic and inorganic types. The most significant *MC* increase occurs with CPAM, negatively impacting press–filtration cake dewatering. Compared to Sun et al. (2023a, 2023b), CPAM underperforms, as its positive charges are neutralized by the anionic surfactant AES rather than soil particle surface charges (Wang et al., 2018). Additionally, the *ZP* index, reflecting fine particle stability, was used to quantify soil surface charges, as shown in Fig. 5f, with *ZP* results aligning well with *TSS* trends.

The phenomena observed in Fig. 5d–f can be attributed to the existence of a threshold dosage for PACL, NPAM, CPAM, and APAM. This is likely due to the dual role of flocculants, which not only promote flocculation but also increase the viscosity of the liquid. In the initial stage, fine soil particles are aggregated into larger flocs through strong adsorption or charge neutralization by flocculant chains, leading to rapid sedimentation and a decrease in *TSS* (Doi et al., 2023; Qin et al., 2023). Simultaneously, the increasing viscosity of the liquid forms a stable suspension system resembling a Newtonian fluid with shear–thinning behavior (Liu et al., 2018), causing *ZP* values to rise. In the second stage, as the flocculant dosage further increases, the molecular chains become widely dispersed in the suspension. This reduces the suspension's rheological properties, decreasing active collisions between flocculant chains and particles (Michał et al., 2022). Although more fine

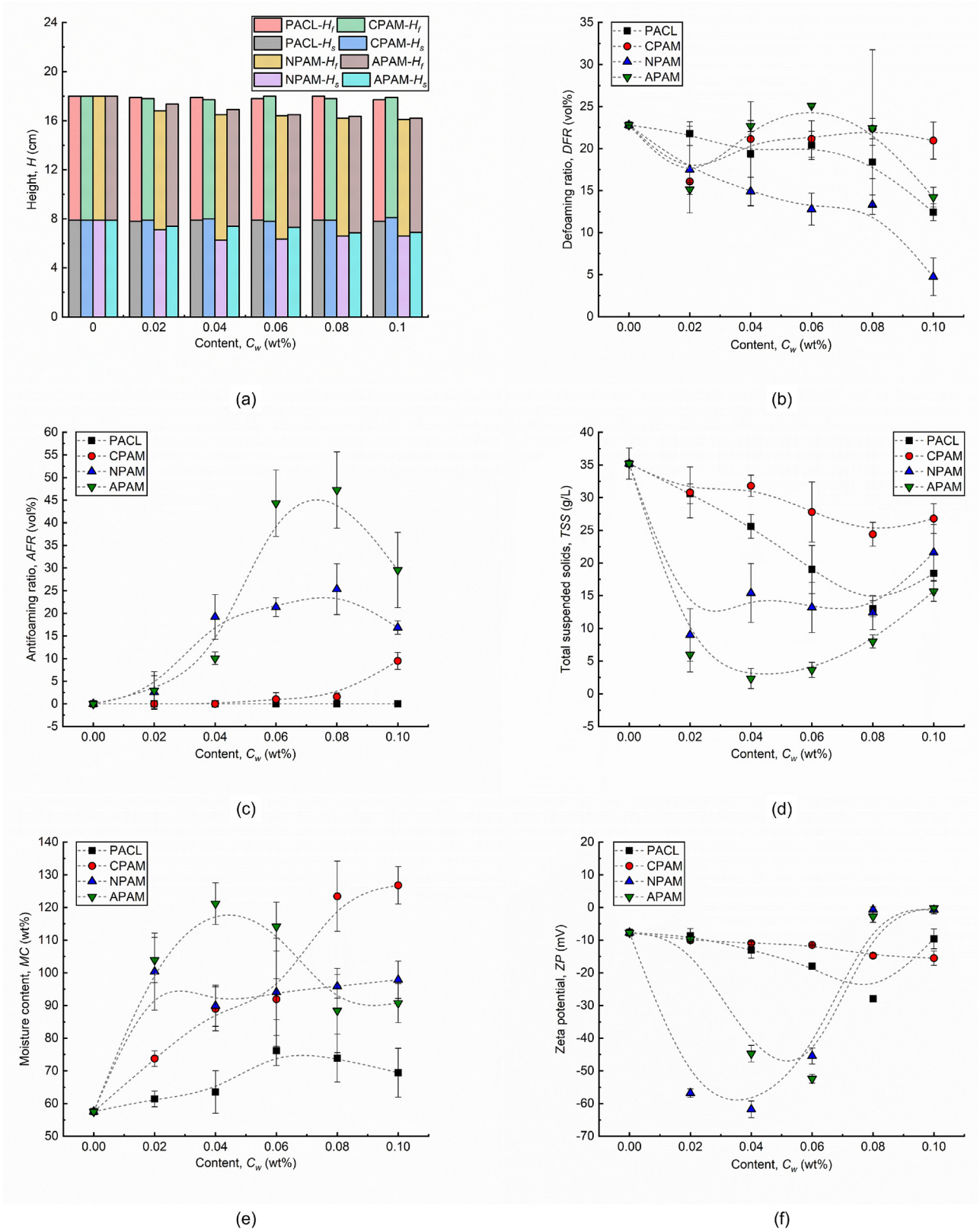

Fig. 5. Variations of defoaming–flocculation–dewatering indices with the concentration and type of flocculants.

particles are adsorbed onto the flocculant chains, the formation of large flocs is hindered, resulting in an increase in *TSS* and *ZP*. This also explains the variation in floc grain size observed in Fig. 9.

4.2. Effects of muck dry mass on defoaming–flocculation–dewatering characteristics

Fig. 6 demonstrates the influence of MDM content ranging from 5 to 30 wt% on defoaming, flocculation, and dewatering performance (30 wt% FC, 0.2 wt% AES, 0.2 wt% APG, 0.02 wt% CMC, 0.002 wt% H–G). Based on a comprehensive evaluation of the parameters presented in Fig. 5, 0.08 wt% PACL (inorganic flocculant) and 0.02 wt% NPAM (organic flocculant) were selected for the study. As depicted in Fig. 6a, the H_f increases from 9.5 to 12.4 cm for PACL with increasing MDM concentration, while a gradual decreasing trend is observed for NPAM. Notably, at 30 wt% MDM with NPAM, the foam–floc–water mixture fails to separate into distinct layers after 2 min of standing, as illustrated in Fig. 6b. Consequently, the H_f value was recorded as the total mixture height in Fig. 6a, and both *DFR* and *AFR* could not be determined, as shown in Fig. 6b and 6c. The experimental results reveal that *DFR* exhibits an increasing trend for PACL but remains relatively constant for NPAM with increasing MDM. Both flocculants demonstrate an initial decrease followed by stabilization in *AFR*, though this trend is more pronounced for NPAM compared to PACL. Regarding foam suppression efficiency, MDM concentrations exceeding a critical threshold or initial moisture content below a certain limit are found to be detrimental. These conditions may result in increased foam volume, challenges in foam–floc separation, or compromised foam inhibition performance.

Similar trends in *TSS* and turbidity for both PACL and NPAM are shown in Fig. 6d and 6e. As MDM increased, *TSS* and turbidity rose, with PACL exhibiting a much more pronounced increase compared to NPAM. The maximum increases in *TSS* and turbidity for PACL reaches 936.30 % and 2474.95 %, respectively, while for NPAM, they are 160.00 % and 61.57 %, respectively. This difference is attributed to the stronger adsorption capacity of NPAM polymer chains compared to PACL, despite PACL's additional charge neutralization effect (Cui et al., 2022; Wei et al., 2018). Conversely, *MC* variations with increasing MDM for PACL and NPAM are nearly opposite due to their differing adsorption behaviors, as illustrated in Fig. 6f. For PACL, *MC* decreases from 133.16 to 58.86 wt% within the 5–20 wt% MDM range and then slightly declines from 58.86 to 56.39 wt% within the 20–30 wt% MDM range. In contrast, for NPAM, *MC* increases from 90.67 to 130.43 wt% within the 5–20 wt% MDM range before decreasing from 130.43 to 113.04 wt % within the 20–30 wt% MDM range, suggesting the existence of a critical *MC* value (also see Fig. 5d–f).

Fig. 7 presents a comparative analysis of the foam–suspension–sediment mixtures at MDM contents of 5 and 30 wt% in the presence of 0.02 wt% NPAM. As illustrated in Fig. 7a, distinct stratification is achieved after standing following stirring, exhibiting a characteristic arrangement comprising an upper foam layer, a middle suspension layer, and a lower sediment layer. However, when the MDM concentration is increased from 5 to 30 wt%, stratification fails to occur within 2 min of standing, as shown in Fig. 7b. This phenomenon can be attributed to the reduced initial water content, which leads to the conversion of nearly all free water into bound water within the flocs. Consequently, bubble ascent is hindered, as evidenced by the visible migration paths of the foams in Fig. 7b. A comparison of Fig. 7a and b further reveals a significant increase in the amount of clay soil particles adsorbed onto the foam film surfaces with higher MDM concentrations. Additionally, the self–healing capacity of the foam liquid films is markedly enhanced as MDM increased. Notably, film rupture consistently occurs through a rapid expansion process of the foams, corroborating the bridging–stretching mechanism (Denkov et al., 2014). The expansion volume of the foam prior to film rupture is substantially greater at 5 wt% MDM compared to 30 wt% MDM, indicating that the adsorption of soil particles strengthens the surface tension of the foams (He et al., 2023).

4.3. Effects of muck fine–grained content on defoaming–flocculation–dewatering characteristics

Fig. 8 demonstrates the influence of FC ranging from 0 to 30 wt% on defoaming, flocculation, and dewatering performance (10 wt% MDM, 0.2 wt% AES, 0.2 wt% APG, 0.02 wt% CMC, 0.002 wt% H–G). Consistent with previous experiments, 0.08 wt% PACL and 0.02 wt% NPAM were employed. As shown in Fig. 8a, the H_f for both PACL and NPAM exhibits minimal variation, although the H_s for PACL is marginally higher than that for NPAM, attributable to its weaker absorptivity. Within the FC range of 0–50 wt%, the *DFR* for both PACL and NPAM shows a gradual increase, with maximum enhancements of 34.16 % and 36.48 %, respectively (Fig. 8b). This improvement can be attributed to the enhanced hydrophobicity of active fine particles imparted by surfactants and polymers, which function as defoaming agents (Denkov et al., 2014). Furthermore, as depicted in Fig. 8c, the AFR remains near 0 for PACL across all tested FCs. In contrast, the AFR for NPAM initially increases, reaching a peak of 6.85 vol% at 30 wt% FC, before declining to 0.63 vol% at higher contents.

Increasing FC results in a significant increase in *TSS* and turbidity for PACL, as depicted in Fig. 8d and 8e. The maximum increases in *TSS* and turbidity are 76.14 % and 33.95 %, respectively. For NPAM, *TSS* and turbidity initially rise to peaks of 9 g/L and 2.49×10^3 NTU within the 0–20 wt% FC range, respectively, before

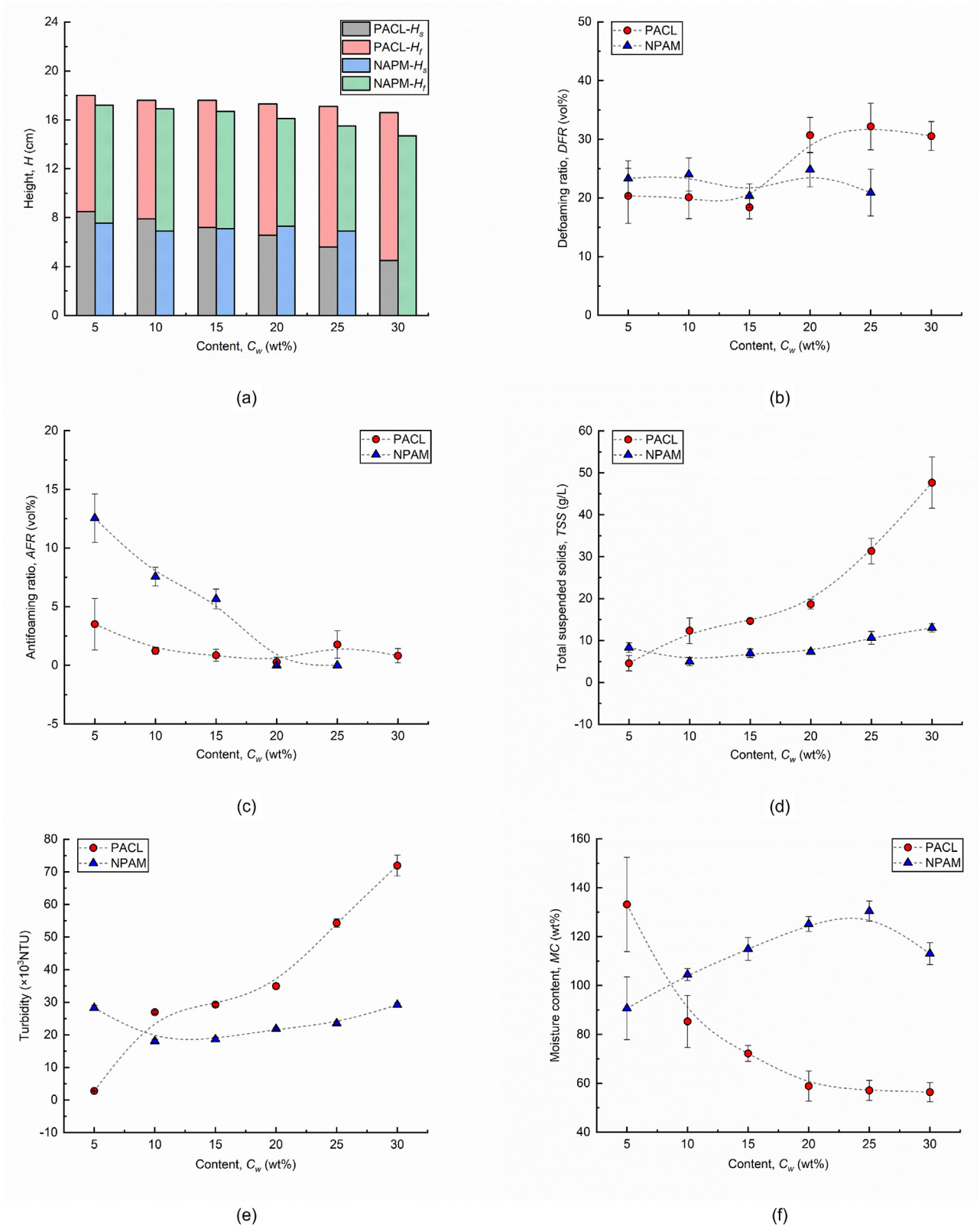

Fig. 6. Variation of defoaming–flocculation–dewatering indices with MDM of EPB shield muck.

declining to 6 g/L and 0.56×10^3 NTU at 50 wt% FC. The upward trends in *MC* with increasing FC for both PACL and NPAM are illustrated in Fig. 8f. Notably, the *MC* for NPAM consistently exceeds that of PACL. Within the 0–50 wt% FC range, the maximum enhancements in *MC* for PACL and NPAM are 30.80 % and 48.55 %,

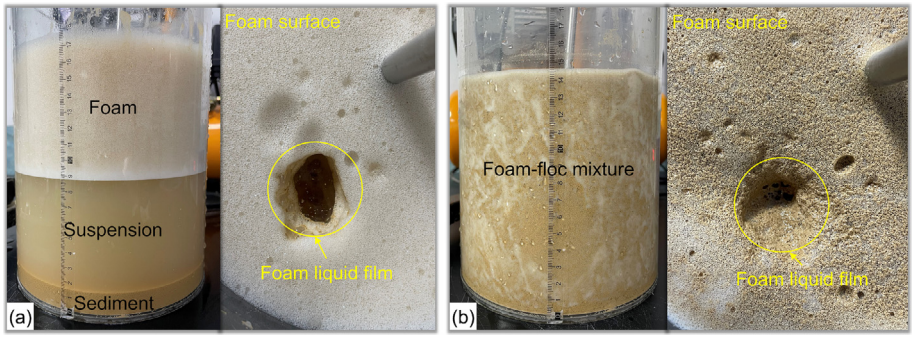

Fig. 7. Visual observation of foam–suspension–sediment mixtures with NPAM: (a) 5 wt% MDM, (b) 30 wt% MDM.

respectively. This phenomenon is primarily attributed to the greater absorption of bound water by clay soils within the electrical double layer compared to hydrophobic sands (Zhang and Pei, 2021).

4.4. Microstructure analysis results

The grain size distributions of PACL and NPAM under different dosages are illustrated in Fig. 9. Upon adding the flocculant, the average floc sizes (Ave) for both PACL and NPAM initially decrease. This is attributed to the broad grain size distribution in the absence of flocculants, which leads to repulsive collisions between particles due to surface charges, Brownian diffusion, fluid motion, and differences in sedimentation rates (Michał et al., 2022). As the dosage increases, collisions transition into active interactions between soil particles and polymer chains, causing the Ave values to rise to a peak. Peak floc sizes of 1761 nm for PACL and 3108 nm for NPAM are achieved at dosages of 0.04 wt% and 0.08 wt%, respectively. The subsequent decline in floc sizes is consistent with the trends observed in Fig. 5d–f, likely due to soil particle surface charge saturation and increased suspension viscosity. Additionally, floc size uniformity improves with higher flocculant dosages. This can be attributed to the increased viscosity of the suspension, which slows the settling rate of soil particles, providing more time for particles to fully interact with flocculant molecules, as clarified in section 4.1. Notably, the floc size frequency reaches 100 % when the PACL dosage exceeds 0.06 wt%. The floc sizes achieved with NPAM are significantly larger than those with PACL, reflecting NPAM's stronger adsorption capacity for soil particles and bound water. These results align with the findings of Wang et al. (2019), further confirming PACL's superior filterability and dewaterability compared to NPAM, as demonstrated in Fig. 5e.

Fig. 5 demonstrates comparable trends in the defoaming–flocculation–dewatering behavior of NPAM and APAM across varying dosages. To elucidate the subtle microstructural differences, SEM images of the press–filtration cakes are presented in the same figure. In the absence of flocculants, the press–filtration cakes exhibited a characteristic stacked texture typical of granite residual soil particles (Hu et al., 2022). The surfaces are rough and porous, with virtually no flocs observed, as depicted in Fig. 10a.

At a magnification of 10,000x, two primary microstructural features are identified for both NPAM and APAM, as shown in Fig. 10b and 10c. Firstly, the polymers absorbed within the flocs form a transparent film upon drying, which progressively obscures the original stacked texture of the soil particle aggregates. As the dosage increases, the polymer film's covering effect become more pronounced, with an accompanying increase in film thickness. This results in a smoother and denser surface morphology of the filter-press cakes. Notably, at a concentration of 0.02 wt%, the APAM flocs exhibits a higher degree of polymer film coverage compared to NPAM flocs, which correlates with the lower *TSS* values observed for APAM in Fig. 5d. Secondly, an increase in the flocculant dosage leads to a greater number of floc structures adhering to the cake surfaces. From this perspective, the distinction between NPAM and APAM flocs is not markedly evident. The SEM imagery provides a clear visual representation of these microstructural alterations, underscoring how variations in flocculant type and dosage significantly affect the dewatering efficiency and the physical properties of the press–filtration cakes.

4.5. Interrelation between flocculation and dewatering indices

Fig. 11 presents the fitting results for the experimental data depicted in Fig. 5d and e. A linear relationship between the flocculation index (*TSS*) and the dewatering index (*MC*) is evident, with a high coefficient of determination (R^2 = 0.80–0.88) and a low root mean square error (*RMSE* = 2.57–10.43), regardless of the flocculant type, including both organic and inorganic variants. *TSS* exhibits a negative correlation with *MC*, indicating that optimal flocculation performance and optimal dewatering performance may not be achieved simultaneously when using flocculants. Consequently, it can be inferred that a relatively optimal dosage should be determined by balancing both flocculation and dewatering effects. Furthermore, the flocculants employed in this study are classified as polymers, which are known for their strong adsorption capacity for clay soil particles and water molecules, as well as their

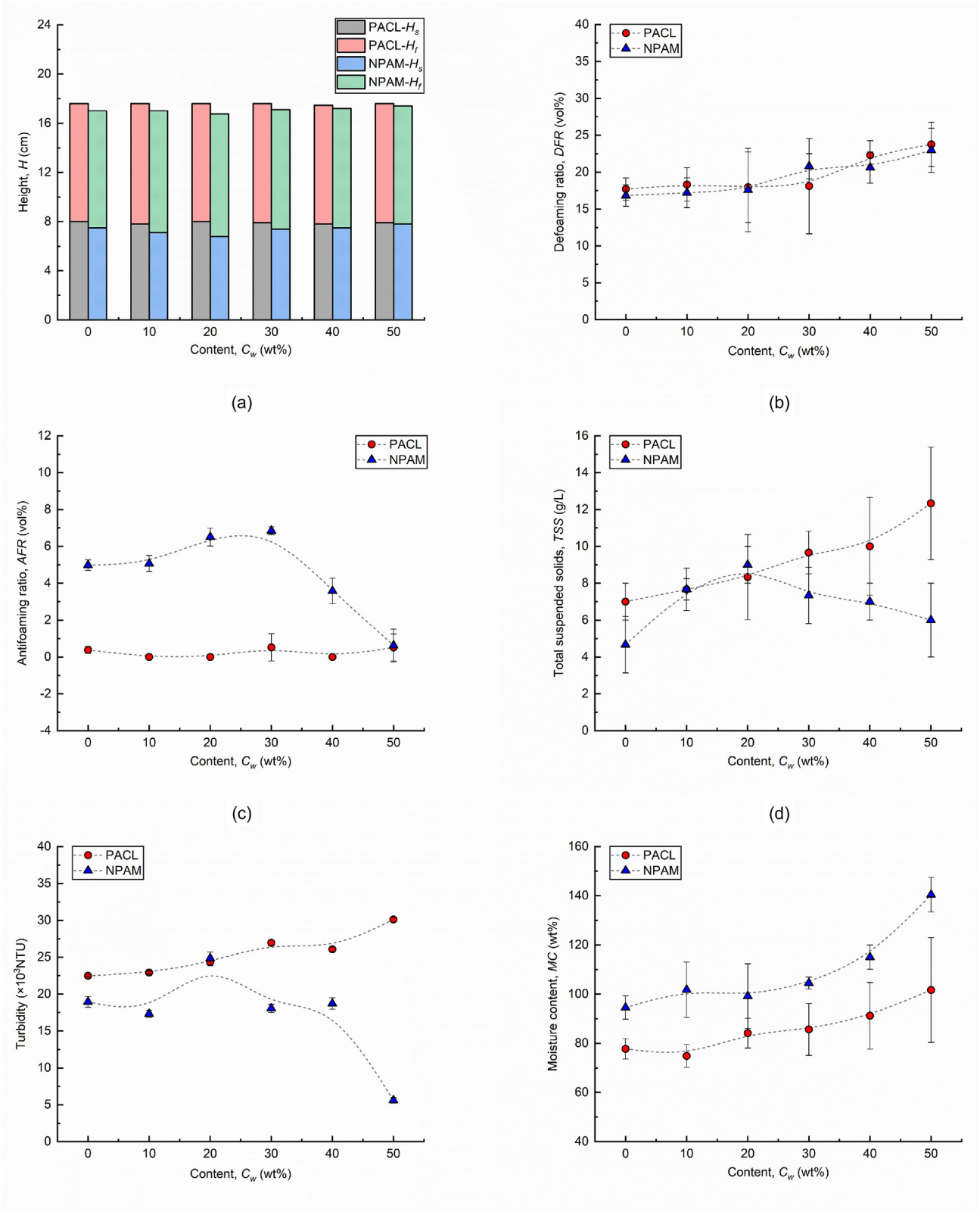

Fig. 8. Variation of defoaming–flocculation–dewatering indices with FC of EPB shield muck.

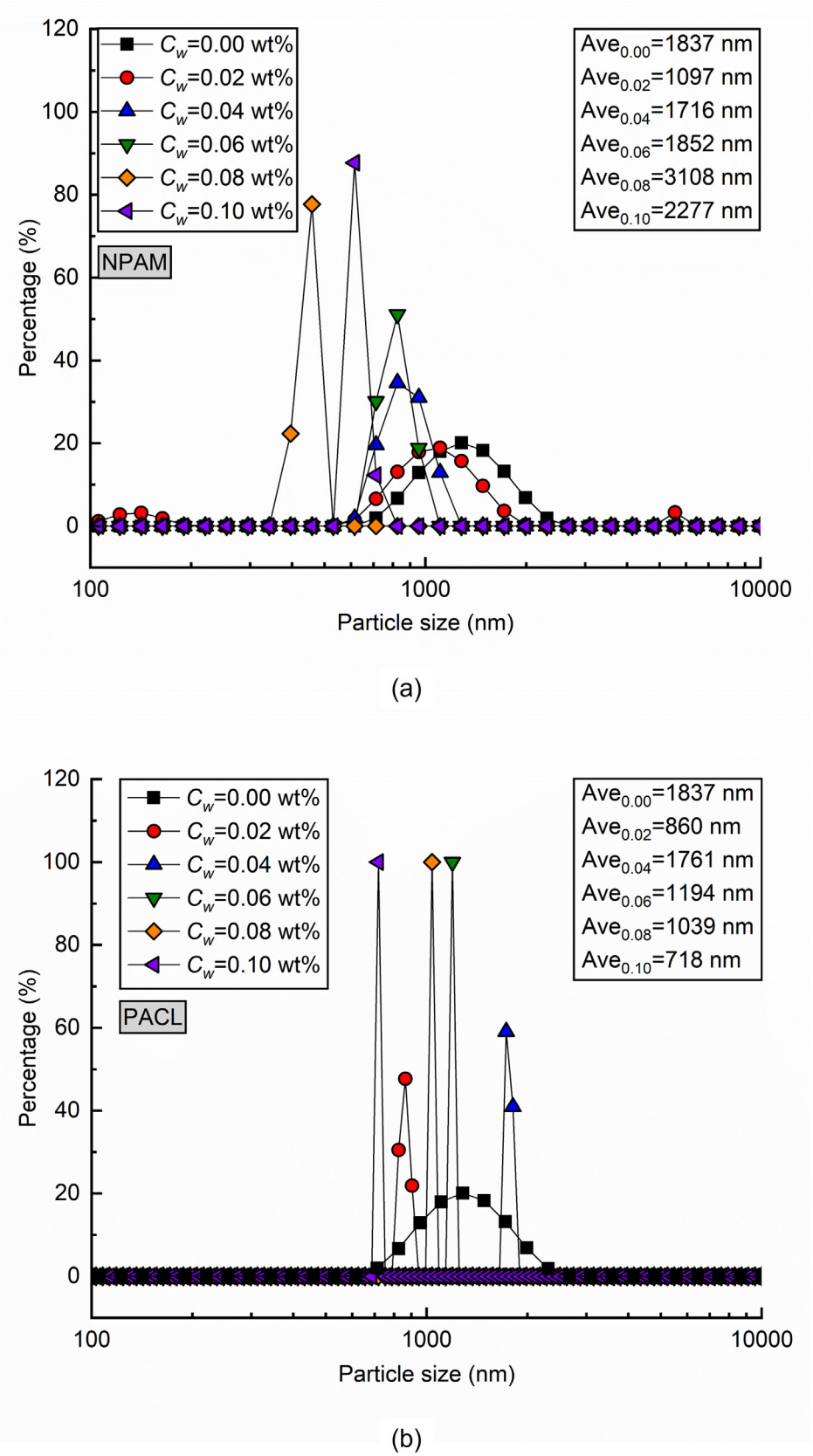

Fig. 9. Grain size analysis of the flocs with the concentration of PACL and NPAM.

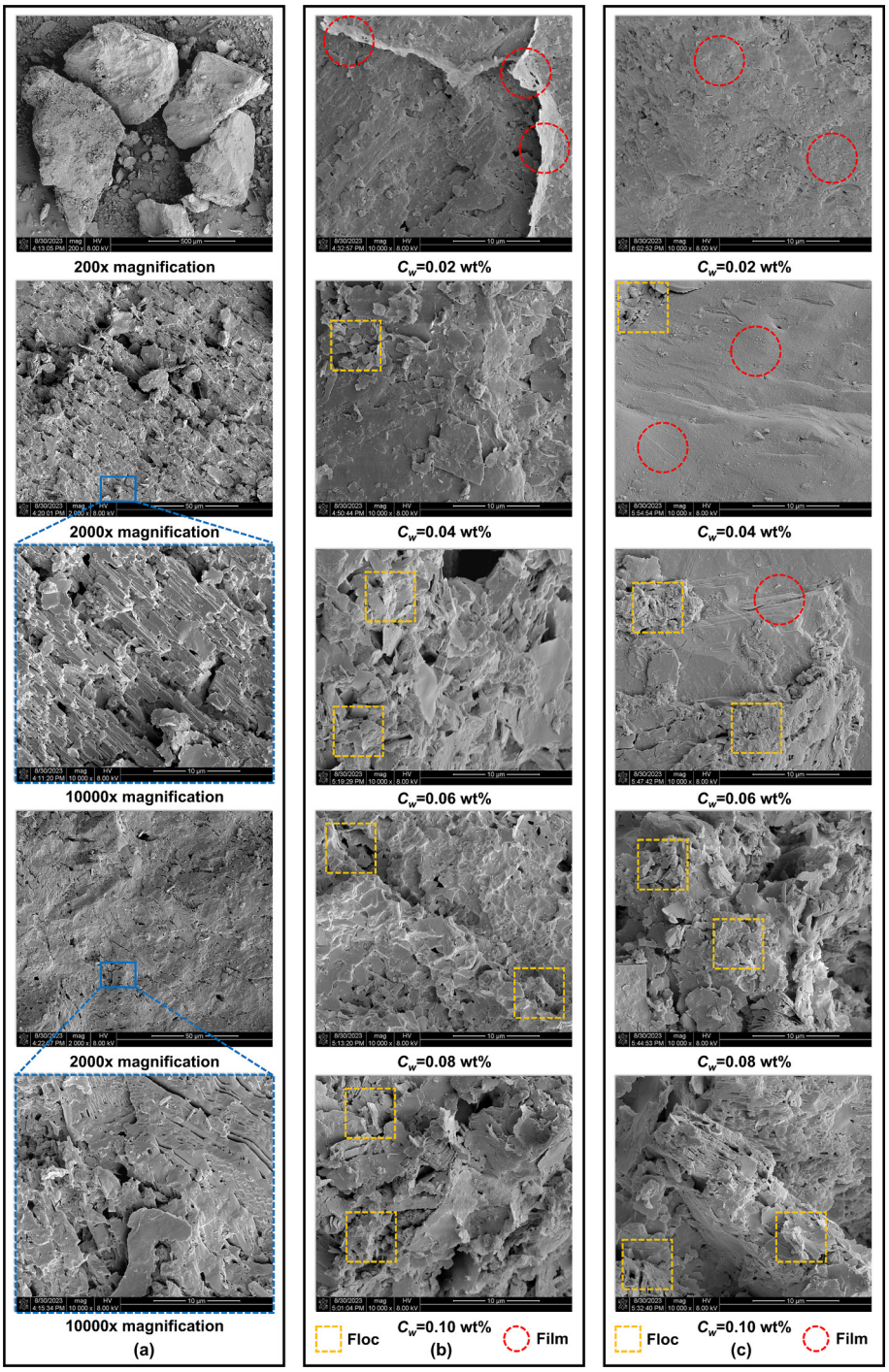

Fig. 10. SEM observations of press–filtration cakes: (a) without flocculant, (b) NPAM and (c) APAM.

charge neutralization capability for soil particle surface charges. These flocculation mechanisms can be further elucidated following the descriptions in Lu et al. (2024d). Thus, the type of flocculant plays a critical role in assessing the in–situ recycling potential of waste EPB shield muck containing residual foams. The geometric features of the four linear expressions, such as slope and line length shown in Fig. 11, provide valuable insights for in–situ recycling practices. For example, CPAM, with the maximum slope (635.53) and the minimum line length among the four flocculants, demonstrates the poorest flocculation and dewatering performance. Specifically, at a given flocculant dosage, a higher flocculation efficiency is associated with a longer line length, while a higher dewatering efficiency is characterized by a smaller slope.

$$R^2 = 1 - \frac{\sum_{i=1}^{n}\left(y_i - y_{ip}\right)^2}{\sum_{i=1}^{n}\left(y_i - y_a\right)^2} \tag{3}$$

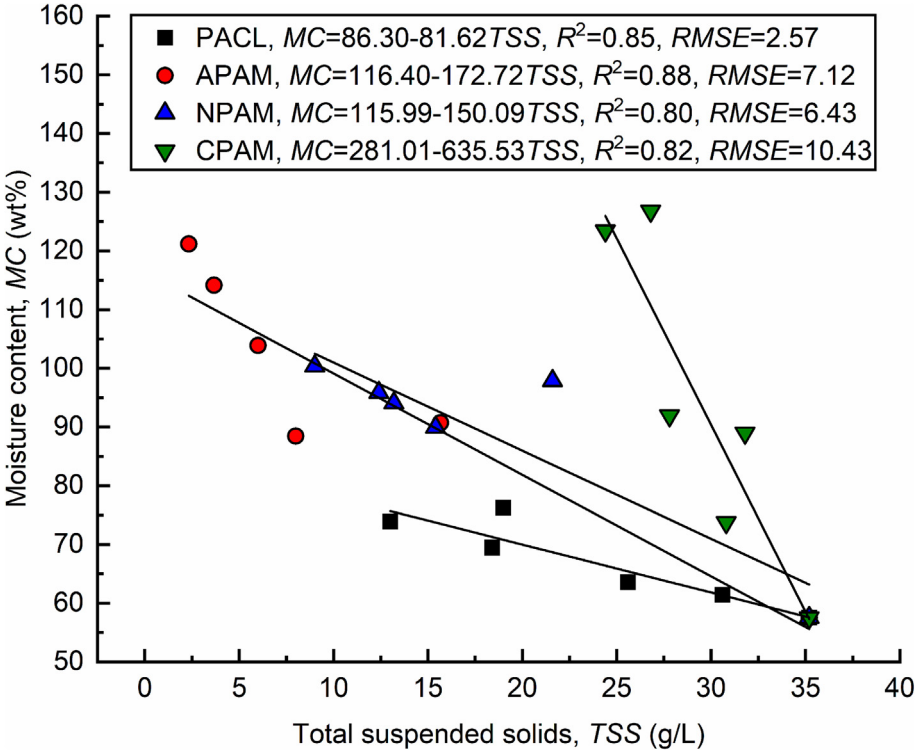

Fig. 11. Correlations between TSS and MC for organic and inorganic flocculants.

$$RMSE = \sqrt{\frac{\sum_{i=1}^{n} \left(y_i - y_{ip}\right)^2}{n}} \quad (4)$$

where y_i is the i–th actual value. y_{ip} is the i–th predicted value. y_a is the mean of the actual values. n is the number of samples.

5. Conclusions

In this study, a series of laboratory experiments were conducted to evaluate the effects of flocculant types, muck dry mass (MDM), and fines content (FC) on the in–situ recycling potential of waste EPB shield muck with residual foams. The key findings are as follows:

(a) NPAM and APAM effectively suppress H_f and H_s while significantly enhancing *AFR*, with NPAM showing the most notable reduction in *DFR*. In contrast, PACL and CPAM have minimal effects on H_f, H_s, *DFR*, and *AFR*. With increasing dosages, *TSS* and *ZP* for PACL, NPAM, and APAM initially rise and then decline, while CPAM shows a continuous upward trend. Due to weakened charge neutralization by anionic surfactants, CPAM is unsuitable for in–situ recycling of shield muck containing foams. The recommended dosages are ≤ 0.02 wt% for APAM and NPAM and approximately 0.08 wt% for PACL at 10 wt% MDM and 30 wt% FC. A linear negative correlation is observed between *TSS* and *MC* for both organic and inorganic flocculants.

(b) Floc grain sizes for PACL and NPAM peak at 1761 nm and 3108 nm, respectively, before decreasing, with grain size distributions becoming more uniform. SEM images reveal that NPAM and APAM form a polymer film on press–filtration cakes, entrapping numerous flocs.

(c) For 0.08 wt% PACL and 0.02 wt% NPAM, PACL enhances H_f, while NPAM gradually reduces H_f with increasing MDM. At 30 wt% MDM, NPAM struggles to separate flocs, foam, and water. PACL significantly improves *DFR*, whereas NPAM more effectively reduces *AFR*. PACL achieves maximum *TSS* and turbidity enhancements of 936.30 % and 2474.95 %, respectively, far exceeding NPAM. *MC* decreases from 133.16 to 56.39 wt% for PACL but increases from 90.67 to 130.43 wt% (at 20 wt% MDM) before declining to 113.04 wt% (at 30 wt% MDM) for NPAM.

(d) Within 0–50 wt% FC, *DFR* for both PACL and NPAM increases with FC, reaching maximum improvements of 34.16 % and 36.48 %, respectively. *AFR* for NPAM is slightly higher than for PACL. With increasing FC, PACL achieves maximum *TSS* and turbidity enhancements of 76.14 % and 33.95 %, respectively. For NPAM, *TSS* and turbidity peak and then decline. *MC* shows an upward trend for both flocculants, with NPAM exhibiting significantly higher values than PACL.

In summary, PACL shows superior dewatering performance compared to NPAM and APAM but exhibits the

lowest efficiency in flocculation and foam suppression. Nevertheless, the optimal dosage of flocculants requires dynamic adjustment depending on the levels of MDM, FC, the composition of foaming agents, and the dosage of defoamers. In future studies, the effects of key mechanical parameters, such as stirring speed and time in the flocculation model apparatus, as well as filtration pressure and time in the pressure–filtration apparatus, on defoaming–flocculation–dewatering behavior should be examined.

CRediT authorship contribution statement

Yao Lu: Writing – review & editing, Writing – original draft, Methodology, Formal analysis, Conceptualization. **Ming Huang:** Resources, Project administration, Funding acquisition. **Jim S. Shiau:** Writing – original draft, Methodology. **Fengwen Lai:** Validation, Methodology, Data curation. **Liqian Peng:** Investigation.

Acknowledgments

This work was supported by the National Youth Top–notch Talent Support Program of China (Grant Nos. 00389335), the National Natural Science Foundation of China (Grant Nos. 52378392), and the "Foal Eagle Program" Youth Top–notch Talent Project of Fujian Province (Grant No. 00387088). Their financial supports are gratefully acknowledged.

References

Acosta-Santoyo, G., Alexandra, R., Bustos, E., Llanos, J., Cañizares, P., Rodrigo, M.A., 2020. Electrochemically assisted dewatering for the removal of oxyfluorfen from a coagulation/flocculation sludge. J. Environ. Manag. 258, 110015.

Budach, C., Thewes, M., 2015. Application ranges of EPB shields in coarse ground based on laboratory research. Tunn. Undergr. Space Technol. 50, 296–304.

Cui, Y.L., Pan, F.R., Zhang, B.B., Wang, X.Q., Diao, H.G., 2022. Laboratory test of waste mud treated by the flocculation–vacuum–curing integrated method. Constr. Build. Mater. 328, 127086.

Denkov, N.D., Marinova, K.G., Tcholakova, S.S., 2014. Mechanistic understanding of the modes of action of foam control agents. Adv. Colloid. Interfac. 206, 57–67.

Doi, A., Nguyen, T.A.H., Nguyen, N.N., Nguyen, C.V., Raji, F., Nguyen, A.V., 2023. Enhancing shear strength and handleability of dewatered clay–rich coal tailings for dry–stacking. J. Environ. Manag. 344, 118488.

GB/T 50145, 2007. Standard for engineering classification of soil. China Planning Press, China.

He, J., Liu, G.Y., Sang, G.C., He, J.H., Wu, Y.H., 2023. Investigation on foam stability of multi–component composite foaming agent. Constr. Build. Mater. 391, 131799.

He, W.P., Luo, J.C., Huang, J.G., Tang, C., Yang, Z., 2024. Two–stage injection of polymer and microsand during ballasted flocculation for treating kaolin waters with or without humic acid: Floc evolutional characteristics, performance and mechanisms. Water Res. 259, 121846.

Hu, Y.X., Yang, D., Li, S.S., Li, H., Zhang, S., Hou, Y.K., Hu, W.Z., Zheng, H., 2022. Preliminary study on preparation of unfired bricks using filter cake from tunnel muck. J. Build. Eng. 60, 105175.

ISO 14688–1, 2017. Geotechnical investigation and testing – Identification and classification of soil – Part 1: Identification and description. The International Organization for Standardization, Switzerland.

ISO 14688–2, 2017. Geotechnical investigation and testing – Identification and classification of soil – Part 2: Principles for a classification. The International Organization for Standardization, Switzerland.

Konig, T.N., Shulami, S., Rytwo, G., 2012. Brine wastewater pretreatment using clay minerals and organoclays as flocculants. Appl. Clay Sci. 67–68, 119–124.

Lai, F.W., Tschuchnigg, F., Schweiger, H.F., Liu, S.Y., Shiau, J., Cai, G. J., 2025. A numerical study of deep excavations adjacent to existing tunnels: integrating CPTU and SDMT to calibrate soil constitutive model. Can. Geotech. J. 62, 1–23.

Li, L.X., Peng, C., Deng, L.H., Zhang, F.G., Wu, D., Ma, F., Liu, Y., 2022a. Understanding the synergistic mechanism of PAM–$FeCl_3$ for improved sludge dewaterability. J. Environ. Manag. 301, 113926.

Li, S.C., Wan, Z.E., Zhao, S.S., Ma, P.F., Wang, M.L., Xiong, B., 2022b. Soil conditioning tests on sandy soil for earth pressure balance shield tunneling and field applications. Tunn. Undergr. Sp. Technol. 120, 104271.

Liu, J., Cheng, Y., Xu, K., An, L.L., Su, Y.H., Li, X.H., Zhang, Z.J., 2018. Effect of nano–silica filler on–microstructure and mechanical properties of polydimethylsiloxane–based nanocomposites prepared by "inhibition–grafting" method. Compos. Sci. Technol. 167, 355–363.

Lu, Y., Huang, M., Huang, P.W., Xu, C.S., Wang, Y., Hu, Y.F., 2024a. Soil conditioning for EPB shield tunneling in coastal silty clay strata: laboratory research and field application. Int. J. Geomech. 24 (2), 04023289.

Lu, Y., Huang, M., Wang, B.N., Zhou, Q., Hu, Y.F., Xue, H.K., 2024b. Efects of residual foaming agent and defoamer on defoaming–focculation–flterpress characteristics of earth pressure balance shield muck. Environ. Sci. Pollut. Res. 31, 43080–43095.

Lu, Y., Huang, M., Zhang, C.Z., Wang, B.N., Peng, L.Q., Wei, W., 2024c. Optimization of defoaming–flocculation–dewatering indices of earth pressure balance (EPB) shield muck using response surface methodology and desirability approach. J. Rock. Mech. Geotech. https://doi.org/10.1016/j.jrmge.2024.04.001.

Lu, Y., Huang, M., Zhou, Q., Wang, B.N., Wei, W., Chen, J., 2024d. On recycling earth pressure balance shield muck with residual foaming agent: defoaming and antifoaming investigations. Environ. Sci. Pollut. Res. 31, 8046–8060.

Michał, H., Marek, O., Andżelika, K., Sylwia, W., Magdalena, M., 2022. A review of flocculants as an efficient method for increasing the efficiency of municipal sludge dewatering: mechanisms, performances, influencing factors and perspectives. Sci. Total Environ. 820, 153328.

Najafabadi, Z.R., Soares, J.B.P., 2021. Flocculation and dewatering of oil sands tailings with a novel functionalized polyolefin flocculant. Sep. Purif. Technol. 274, 119018.

Qin, X.H., Zhou, Z.Q., He, B., Xu, B., Yu, S.L., Qin, G.L., Liu, K., Ma, Y.J., Han, P.J., 2023. Characteristics of waste mud treated by construction waste–slag based flocculation–solidification combined method. Constr. Build. Mater. 370, 130699.

Sun, X.H., Chen, Z.Y., Guo, K.Y., Fei, J.B., Dong, Z.J., Xiong, H., 2023a. Geopolymeric flocculation–solidification of tail slurry of shield tunnelling spoil after sand separation. Constr. Build. Mater. 387, 131569.

Sun, X.H., Chen, Z.Y., Sun, Z.B., Wu, S.L., Guo, K.Y., Dong, Z.J., Peng, Y.S., 2023b. High–Efficiency utilization of waste shield slurry: A geopolymeric Flocculation–Filtration–Solidification method. Constr. Build. Mater. 387, 131569.

Wang, H.F., Hu, H., Wang, H.J., Zeng, R.J., 2019. Combined use of inorganic coagulants and cationic polyacrylamide for enhancing dewaterability of sewage sludge. J. Clean. Prod. 211, 387–395.

Wang, J., Zhao, R., Cai, Y.Q., Fu, H.T., Li, X.B., Hu, X.Q., 2018. Vacuum preloading and electro–osmosis consolidation of dredged slurry pre–treated with flocculants. Eng. Geol. 246, 123–130.

Wang, S.Y., Feng, Z.Y., Qu, T.M., Huang, S., Zheng, X.C., 2023. Effect of water head on the permeability of foam–conditioned sands: Experimental and analytical investigation. Soils Found. 63 (6), 101404.
Wei, H., Gao, B.Q., Ren, J., Li, A.M., Yang, H., 2018. Coagulation/flocculation in dewatering of sludge: a review. Water Res. 143, 608–631.
Wei, Y.J., Yang, Y.Y., Tao, M.J., Wang, D.L., Jie, Y.X., 2020. Earth pressure balance shield tunneling in sandy gravel deposits: a case study of application of soil conditioning. Bull. Eng. Geol. Environ. 79 (9), 5013–5030.
Wu, S.L., Li, X.D., Jiang, P.M., Xu, H.Q., Min, F.L., 2022. Dewatering characteristics of waste slurry from pipe jacking based on improved vacuum filtration method. Tunn. Undergr. Space Technol. 130, 104727.
Yin, Y.P., Li, B., Wang, W.P., Zhan, L.T., Xue, Q., Gao, Y., Zhang, N., Chen, H.Q., Liu, T.K., Li, A.G., 2016. Mechanism of the december 2015 catastrophic landslide at the Shenzhen landfill and controlling geotechnical risks of urbanization. Engineering 2 (2), 230–249.
Zhang, C., Chen, K., Yang, J.S., Fu, J.Y., Wang, S.Y., Xie, Y.P., 2021. Reuse of discharged soil from slurry shield tunnel construction as synchronous grouting material. J. Constr. Eng. Manag. 148 (2), 04021193.
Zhang, C., Yang, J.S., Xie, Y.P., Fu, J.Y., Wang, S.Y., Yin, J., 2022a. Utilization of tunnel spoils as a lightweight filling material for the voids behind tunnel excavation contour. J. Clean. Prod. 372, 133559.
Zhang, C., Yang, J.S., Fu, J.Y., Wang, S.Y., Yin, J., Xie, Y.P., 2020. Recycling of discharged soil from EPB shield tunnels as a sustainable raw material for synchronous grouting. J. Clean. Prod. 268, 121947.
Zhang, R.J., Zheng, Y.L., Dong, C.Q., Zheng, J.J., 2022b. Strength behavior of dredged mud slurry treated jointly by cement, flocculant and vacuum preloading. Acta Geotech. 17 (6), 2581–2596.
Zhang, S.Q., Pei, H.F., 2021. Determining the bound water content of montmorillonite from molecular simulations. Eng. Geol. 294, 106353.
Zhang, T.S., Yuan, J.M., Wang, W., Chen, P.X., Chen, C.F., Wu, X.D., Wei, J.X., Yu, Q.J., 2024. Efficient utilization of waste shield slurry and CDW fines to prepare eco–friendly controlled low–strength material. J. Clean. Prod. 444, 141343.
Zhang, Y.J., Wang, J., Zhang, L.L., Li, C.L., Jiang, H., Ba, X.Z., Hou, D. S., 2022c. Study on the preparation and properties of high–belite cementitious materials from shield slag and calcium carbide slag. Constr. Build. Mater. 355, 129082.
Zhou, S.H., Li, X., Ji, C., Xiao, J.H., 2017. Back–fill grout experimental test for discharged soils reuse of the large–diameter size slurry shield tunnel. KSCE J. Civ. Eng. 21 (3), 725–733.